

# Stochastic approximation analysis of dynamical quantum critical phenomena in long-range transverse-field Ising chain

Sora Shiratani\*

*Department of Physics, The University of Tokyo, Tokyo 113-0033, Japan*

Syngé Todo†

*Department of Physics, The University of Tokyo, Tokyo 113-0033, Japan*

*Institute for Physics of Intelligence, The University of Tokyo, Tokyo 113-0033, Japan and*

*Institute for Solid State Physics, The University of Tokyo, Kashiwa, 277-8581, Japan*

(Dated: May 24, 2023)

The quantum phase transition of the long-range transverse-field Ising model is explored by combining a quantum Monte Carlo method with the optimal computational complexity scaling and stochastic parameter optimization that renders space and imaginary time isotropic, specifically achieved by tuning correlation lengths. Varying the decay rate of the long-range interaction, we exhaustively calculate the dynamical critical exponent and the other exponents precisely in mean-field, nonuniversal, and Ising universality regimes. In our simulations, critical properties are extracted only from a set of simulations with different  $L$ , significantly improving computational cost compared to the standard finite-size scaling approach based on data collapse. We also perform a hypothesis test at the predicted universality boundary, which supports preceding reports arguing that conventional theoretical prediction fails to locate the universality boundary.

## I. INTRODUCTION

Long-range interacting systems have been a subject of interest in statistical physics for decades, and enormous efforts have gradually revealed their rich nature. Historically, long-range systems have been studied mainly from theoretical viewpoints [1–9], but recently the situation has been changing; Due to improvements in experimental techniques, they are no longer a figment of the imagination: long-range systems appear in spin-ice materials [10, 11], quantum optics [12–18], Rydberg atoms [19–23], etc. In addition, massive advance in computational physics from both algorithm and hardware sides has also empowered us to investigate long-range systems numerically in detail [24–43]. Modern research on long-range systems has been speeding up, fueled by these developments.

Among many rich properties of long-range interacting systems, quantum phase transition (QPT) under strong space-time anisotropy would be one of the most intriguing and challenging phenomena. In quantum long-range interacting systems, spatial (long-range) interaction and temporal (short-range) one give rise to extreme anisotropy, and by varying the degree of long-range nature, one can observe continuously changing critical behavior accompanied by changes of universality class. Given this property, one would naturally be tempted to perform a detailed simulation across different universality classes in a coherent manner. Needless to say for the theoretical approach, it is also challenging for numerical simulations.

Initially, conventional simulation techniques for QPT, such as DMRG [44] and quantum Monte Carlo (QMC) [45], are dedicated to short-range systems. Now, however, they are also applicable to them without any computation penalty compared to short-range cases, thanks to advanced tricks such as matrix product operator [46, 47] or Poisson process thinning [48, 49]. But still, to extract critical exponents, we had to rely on traditional finite-size scaling (FSS) analysis [50–52], for which we have to accumulate numerical data for exhaustive parameter sets by consuming considerable computational resources. The computational cost problem is particularly prominent in the case of QMC, leading to a dilemma that we have to give up either the statistical exactness of QMC or the coverage of parameter space. To perform a detailed simulation without compromise, we need a QMC-based scheme that does not rely on FSS.

In this paper, we analyze the ferromagnetic long-range transverse-field Ising model with algebraic interaction  $J_{ij} \propto 1/|i - j|^{1+\sigma}$  by a new approach that combines long-range QMC [48] with stochastic parameter optimizer [53, 54]. In our simulations, only the decay rate  $\sigma$  and the system size  $L$  are the input parameter, and the inverse temperature  $\beta$  and the transverse field  $\Gamma$  are not:  $\beta$  and  $\Gamma$  are automatically tuned so that the system is at the quantum critical point being the real space and the imaginary time isotropic. This procedure forces observables to obey a power law regarding system size  $L$ , and scaling powers are directly linked to critical exponents [41, 54, 55]. Namely, we can extract critical properties only from a set of simulations with different  $L$ , enabling us to perform exhaustive simulations over several tens of different decay rates  $\sigma$ 's across three distinct universality classes as shown in Fig. 1.

This paper is organized as follows; In Sec. II, we survey previous results on the long-range transverse-field Ising

\* sora.shiratani@phys.s.u-tokyo.ac.jp

† wistaria@phys.s.u-tokyo.ac.jp

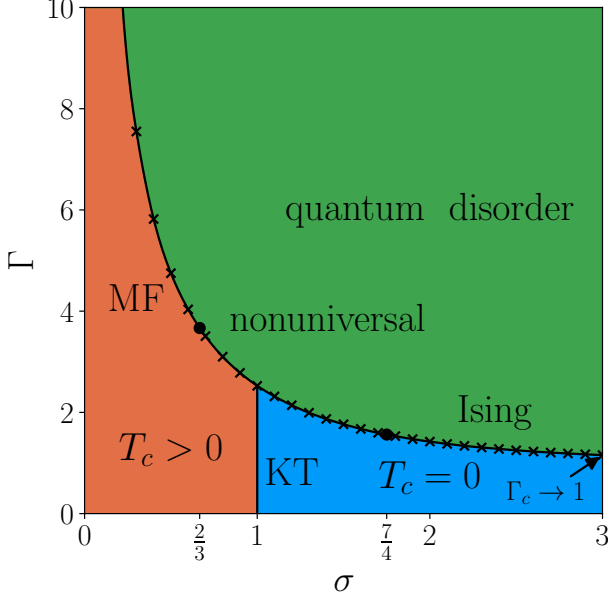


FIG. 1. Zero-temperature phase diagram of the long-range transverse-field Ising model. The curve, which corresponds to  $\Gamma_c$ , is the cubic spline interpolation of data points at  $\sigma = 0.1, 0.2, \dots, 3.0$  ( $\times$  symbols,  $\Gamma_c(0.1), \Gamma_c(0.2)$  are outside the range). For  $\sigma \leq 2/3$ ,  $2/3 \leq \sigma \leq 7/4$ ,  $7/4 \leq \sigma$ , the quantum phase transition is classified as the mean-field, nonuniversal, and Ising universality classes, respectively. At  $\sigma = 1$ , the Kosterlitz-Thouless transition divides the finite-temperature ordered phase and the disordered phase [8, 9, 38, 43, 48, 56, 57].

model, focusing on theoretical aspects. In Sec. III, we elaborate on our tuning scheme. More details, including the QMC sampling scheme and heuristics for parameter optimization, will be described in the Appendix. In Sec. IV, the results are shown in two parts: direct analysis achieved by two-parameter optimization and hypothesis testing for universality boundary determination, which uses predecided  $\beta$ . Finally, in Sec. V, we discuss the results and conclude this paper.

## II. THEORETICAL BACKGROUND

### A. model

The Hamiltonian of the ferromagnetic long-range transverse-field Ising model (LRTFIM) is defined as follows:

$$H = - \sum_{i < j} \frac{1}{|i - j|^{1+\sigma}} \hat{\sigma}_i^z \hat{\sigma}_j^z - \Gamma \sum_i \hat{\sigma}_i^x, \quad (1)$$

where  $i, j \in \mathbb{Z}_{[1, L]}$  each labels particular spin on  $L$ -site one-dimensional periodic chain,  $\hat{\sigma}_i^x$  and  $\hat{\sigma}_i^z$  are the Pauli matrices operate on site  $i$ ,  $\sigma$  is the decay rate of pairwise

interactions and  $\Gamma$  is the transverse field. To ensure the extensivity of the energy,  $\sigma$  must be positive. Otherwise,  $\langle H/L \rangle$  diverges in the thermodynamic limit [58, 59]. In our simulations, the bare interaction  $\frac{1}{|i-j|^{1+\sigma}}$  is corrected by bundling all the interactions between infinite mirrors  $(i, j + LZ)$  to a single  $J_{ij}$  [5, 37, 60] to reduce finite-size artifacts. For the one-dimensional case, the corrected sum  $\sum_{n \in \mathbb{Z}} \frac{1}{|i-j+nL|^{1+\sigma}}$  ( $i, j \in \mathbb{Z}_{[1, L]}$ ) is expressed by the Hurwitz zeta function  $\zeta(s, q) = \sum_{n=0}^{\infty} \frac{1}{(q+n)^s}$ , i.e., we get

$$J_{ij} = \frac{1}{L^{1+\sigma}} \left[ \zeta \left( 1 + \sigma, \frac{|i-j|}{L} \right) + \zeta \left( 1 + \sigma, 1 - \frac{|i-j|}{L} \right) \right] \quad (2)$$

as effective interaction.

To sum up, the model of interest is

$$H = - \sum_{i < j} J_{ij} \hat{\sigma}_i^z \hat{\sigma}_j^z - \Gamma \sum_i \hat{\sigma}_i^x. \quad (3)$$

At  $T = 0$ , the quantum phase transition (QPT) is predicted to occur [55, 56]; For large  $\Gamma$ , its ground state is a polarized state aligned along the  $x$ -axis, while for small  $\Gamma$ , it is an Ising-like ferromagnet. The order parameter of this QPT is the squared magnetization along the  $z$ -axis,  $m^2 = \left[ \frac{1}{L} \sum_i \sigma_i^z \right]^2$  [55, 61].

### B. theoretical predictions

In this section, we briefly review the theoretical predictions based on the mean-field theory. The effective action of the LRTFIM is the same as the  $(1+1)$ -dimensional Ising model up to an additional term  $\propto q^\sigma$  accounting for the long-range interactions. To be more specific, we obtain the following action [36, 56]:

$$\iint dq d\omega \tilde{\phi}^* \tilde{G}(q, i\omega)^{-1} \tilde{\phi} + \iint dx d\tau \frac{u}{4!} \phi^4, \quad (4)$$

where  $\phi = \phi(x, \tau)$  is a field defined on the  $(1+1)$ -dimensional space,  $\tilde{\phi} = \tilde{\phi}(q, i\omega)$  is the Fourier transform of  $\phi$ ,  $\tilde{G}(q, i\omega)^{-1} = \omega^2 + q^2 + cq^\sigma + d$  is a long-ranged Gaussian propagator, where  $c > 0$  is a constant and  $d \propto \Gamma - \Gamma_c$  is a mass term.

For  $\sigma \geq 2$ , the singularity of the propagator at  $\Gamma = \Gamma_c$  is governed by  $\omega^2$  and  $q^2$ ; It means that the system is effectively the same as the isotropic two-dimensional Ising model, and thus the criticality is described by the well-known Ising critical exponents [62, 63] (see Table I). This result is well tested by various approaches [1, 3, 7, 27, 32, 56, 64–67]. However, it is also stated that the lower bound of the Ising universality decreases to  $7/4$  due to higher-order contributions, and this observation is also well supported [4, 36, 68–75]. For a while, let us assume that the Ising universality appears for  $\sigma \geq 2$ . We will revisit this topic later.

For  $\sigma < 2$ , the singularity is now dominated by  $\omega^2$  and  $q^\sigma$ ; The critical exponents can be nontrivial, and anisotropy of  $\omega$  and  $q$  leads to the dynamical exponent  $z$ , which is known as a barometer of anisotropy, being different from unity. It is still possible to calculate mean-field critical exponents provided the criticality is described by the corrected Gaussian fixed point (see Table I for details), however, justification of the assumption is not straightforward. To cope with the difficulty, the lowest-order approximation for the LRTFIM can be compared with its short-ranged counterpart with a fractional spatial dimension  $d_{\text{virtual}} = \frac{2(d+z)}{\sigma}$  [36]. As the upper critical dimension of the classical Ising model is 4, it would be reasonable to conclude that the mean-field universality appears for  $\sigma \leq \frac{2d}{3} = \frac{2}{3}$ . Near the boundary, multiplicative log corrections are predicted [26, 56]. This regime requires extra care in analysis, since the  $\phi^4$  coupling constant  $u$  is a dangerous irrelevant variable [37, 51, 52, 76, 77]. Due to the singularity of free energy at  $u = 0$ , exponents get corrections, and thus we have to get rid of the extra terms to extract bare exponents.

For the remaining  $\frac{2}{3} < \sigma < 2$ , exponents are nontrivial in the true sense; At present, analyses are mainly based on numerical approaches such as series expansion [24, 26], exact diagonalization [27–35], tensor network [32, 78, 79], functional RG [36] and quantum Monte Carlo [37–43].

Although it is out of the scope of this paper, it is known that for  $\sigma < 1$ , a finite-temperature phase transition exists in addition to the QPT we are focusing on. The ordered phase abruptly disappears at  $\sigma = 1$  via the Kosterlitz-Thouless phase transition [8, 9, 38, 43, 48, 56, 57] as in Fig. 1.

symbol	MF ( $\sigma \leq \frac{2}{3}$ )	Ising ( $2 \leq \sigma$ )
$\beta$	$\frac{1}{2} - \frac{\sigma}{4}$	$\frac{1}{8}$
$\gamma$	1	$\frac{7}{4}$
$\nu$	$\frac{1}{\sigma}$	1
$z$	$\frac{\sigma}{2}$	1

TABLE I. Table of the critical exponents.

### C. critical exponents

In the vicinity of quantum critical point, several observables show distinctive power-law behaviors, and associated critical exponents are defined [55]. As the QPT occurs at  $T = 0$ , the degrees of singularity is measured in terms of a control parameter  $g$  rather than shifted temperature  $t = T - T_c$ ; For the LRTFIM,  $g$  is shifted transverse field  $\Gamma - \Gamma_c$ . Aside from this difference, definitions are quite similar to classical counterparts:  $\beta$  is defined from squared magnetization  $m^2 \sim g^{2\beta}$ ,  $\gamma$  from susceptibility  $\chi \sim 1/g^\gamma$  and  $\nu$  from correlation length  $\xi \sim 1/g^\nu$ . Additionally, quantum-specific exponent  $z$  (also known as the dynamic critical exponent) is defined from corre-

lation length along the imaginary-time axis  $\xi_\beta \sim 1/g^{z\nu}$ . Note that this section specializes in the  $L = \infty$  case.

### D. finite-size scaling

Let  $Q$  be a physical quantity, parametrized by system size  $L$ , shifted temperature  $t$ , and field  $g$ . As long as  $(t, g)$  is sufficiently close to the critical point  $(0, 0)$ , we can make use of the following finite-size scaling relation for  $b \geq 1$  [54]:

$$Q(L, t, g) = b^{-x_Q} Q(b^{-1}L, b^{x_t}t, b^{x_g}g), \quad (5)$$

where  $(x_Q, x_t, x_g)$  is scaling dimensions of corresponding parameters. In contrast to  $x_Q$  being unknown in general,  $(x_t, x_g)$  can be rewritten as  $(z, 1/\nu)$  where  $(z, \nu)$  are critical exponents of correction lengths (see Sec. II C) [55]. Since  $b \geq 1$  is arbitrary, we can safely set  $b = L$ . Finally, we get

$$Q(L, t, g) = L^{-x_Q} Q(tL^z, gL^{1/\nu}). \quad (6)$$

Note that we dropped the first argument by redefining  $Q(a, b) = Q(1, a, b)$ .

### E. optimization and scaling relation

In our simulations, we specifically rely on Eq. (6) for  $\xi/L$  and  $\xi_\beta/\beta$ :

$$Q_1(tL^z, gL^{1/\nu}) = \frac{\xi(L, t, g)}{L}, \quad (7)$$

$$Q_2(tL^z, gL^{1/\nu}) = \frac{\xi_\beta(L, t, g)}{\beta}. \quad (8)$$

For those cases, two  $x_Q$  are trivially zero. Of course, two  $Q$  are still unknown. Actually, we do not even evaluate  $Q$ : we exploit their parameter dependencies only. As we have two formulae and two variables  $(tL^z, gL^{1/\nu})$ , if we set  $(tL^z, gL^{1/\nu}) = \text{const.}$  then Eq. (7) and Eq. (8) are constant, and vice versa. Namely, we can coerce  $(tL^z, gL^{1/\nu})$  into some constants by imposing

$$\frac{\xi(L, t, g)}{L} = R, \quad (9)$$

$$\frac{\xi_\beta(L, t, g)}{\beta} = R, \quad (10)$$

where  $R > 0$  is some arbitrary constant and  $(t, g) = (t(L), g(L))$ . While we set two  $R$  equal with space-time isotropy in mind, they can be different in principle. For later convenience, let us rewrite Eq. (9) and Eq. (10) as

$$S(0, 0) - [1 + (2\pi R)^2] S\left(\frac{2\pi}{L}, 0\right) = 0, \quad (11)$$

$$S(0, 0) - [1 + (2\pi R)^2] S\left(0, \frac{2\pi i}{\beta}\right) = 0, \quad (12)$$

where  $S(q, i\omega) = \left\langle \frac{1}{L\beta} \left| \sum_i \int_0^\beta e^{iqx+i\omega\tau} \sigma_i^z(\tau) d\tau \right|^2 \right\rangle$  is canonical structure factor. In the equations, two  $\xi$  are replaced by more explicit expressions [80]:

$$\xi = \frac{L}{2\pi} \sqrt{\frac{S(0, 0)}{S(\frac{2\pi}{L}, 0)}} - 1, \quad (13)$$

$$\xi_\beta = \frac{\beta}{2\pi} \sqrt{\frac{S(0, 0)}{S(0, \frac{2\pi i}{\beta})}} - 1. \quad (14)$$

It is remarkable that this procedure nullifies parameter dependence of any scaling function  $Q(tL^z, gL^{1/\nu})$ ; As long as  $\xi/L$  and  $\xi_\beta/\beta$  are fixed at some predefined constant  $R$ , we can directly access to  $x_Q$  through the relation  $Q(L, t, g) \sim L^{-x_Q}$ . In our analyses, we use the following four formulae:

$$\beta(L) \sim L^z, \quad (15)$$

$$\Gamma(L) - \Gamma_c \sim L^{-1/\nu}, \quad (16)$$

$$m^2(L) \sim L^{-2\beta/\nu}, \quad (17)$$

$$\chi(L) \sim L^{\gamma/\nu}. \quad (18)$$

Additionally, in the verification of the hyperscaling relation we combine these equations as  $S(0, 0)/(\beta m^2) \sim L^{2\beta/\nu + \gamma/\nu - z}$  to directly access to  $2\beta/\nu + \gamma/\nu - z$ . Note that the exponents are multiplied by  $-1/\nu$  because their divergences are measured in terms of  $L \propto \xi \sim g^{-1/\nu}$  rather than  $g$ , and four symbols are parametrized solely by  $L$ .

### III. METHOD

#### A. overview

In short, our method consists of two components, i.e., Markov chain Monte Carlo (MCMC) sampler and parameter optimizer, interacting mutually as Fig. 2.

The former holds a microscopic spin state  $\{\sigma_i^z(\tau) \mid i \in \mathbb{Z}_{[1, L]}, \tau \in [0, \beta], \sigma^z \in \{\pm 1\}\}$  drawn from the canonical ensemble and measures  $S(0, 0)$ ,  $S(\frac{2\pi}{L}, 0)$ ,  $S(0, \frac{2\pi i}{\beta})$ , etc. To accelerate sampling, we prepared many equivalent samplers distributed among CPUs and calculated required thermal averages using inter-process broadcasting.

The latter accepts  $S$  sampled by MCMC and applies feedbacks to  $(\beta, \Gamma)$  so that they asymptotically converge to  $(\beta(L), \Gamma(L))$ : the simultaneous root of Eq. (9) and Eq. (10). As  $(\beta, \Gamma)$  quickly approach the root, we can accurately estimate  $(\beta(L), \Gamma(L))$  even from limited samples.

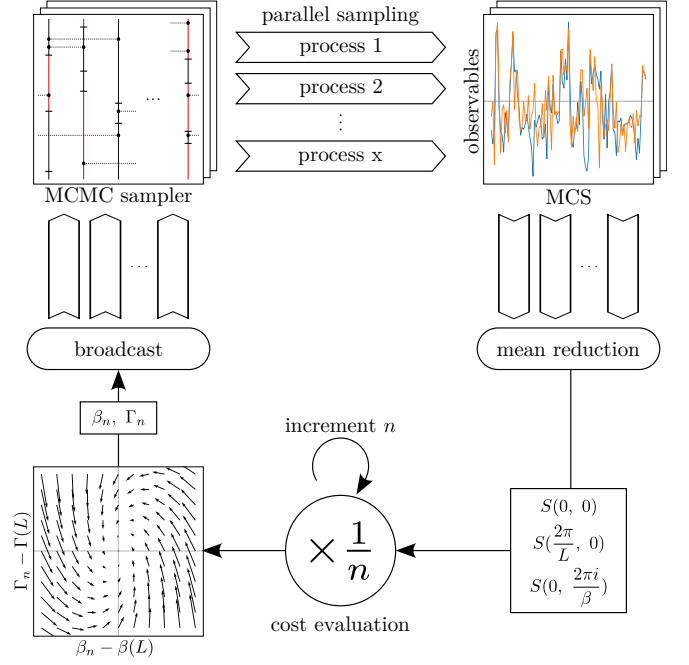


FIG. 2. Schematic representation of the whole process. Each iteration begins with the MCMC step, which samples necessary observables from the canonical ensemble. To increase throughput, this step runs in parallel on multiple processes sharing the same  $(\beta, \Gamma)$ . After that, inter-process averages of the canonical structure factors  $S(0, 0)$ ,  $S(\frac{2\pi}{L}, 0)$ ,  $S(0, \frac{2\pi i}{\beta})$  are calculated to estimate the left hand sides of Eq. (11) and Eq. (12). The optimizer then decides the next  $(\beta, \Gamma)$  so that they approach the root  $(\beta(L), \Gamma(L))$  and distributes them to the parallel samplers. In the bottom left figure, the vector field symbolically represents the “flow” of  $(\beta, \Gamma)$ . To ensure convergence, feedback strength is gradually decreased as  $\propto \frac{1}{n}$  where  $n$  is the number of iterations.

#### B. sampling scheme

First of all, we need a method for calculating canonical structure factor  $S$ . While there are several different realizations, we chose MCMC.

From the methodological view of point, we have trouble here; Since the LRTFIM has  ${}_LC_2 = \mathcal{O}(L^2)$  nonzero interactions, each Monte Carlo step (MCS), i.e., sequence of tasks required for drawing one sample from the canonical ensemble, takes  $\mathcal{O}(L^2)$  time if naively implemented. Counterintuitively, the computational cost can actually be reduced to the optimal scaling  $\mathcal{O}(L)$  with careful treatments [48]. In the algorithm, all the interactions  $J_{ij}$  and even the transverse field  $\Gamma$  are collectively taken into account. For more details, see Appendix.

#### C. parameter tuning algorithm

For parameter tuning, we adopted the Robbins-Monro algorithm [53]. Formally speaking, this algorithm en-

ables us to approximate the root of a monotonic function  $f(\theta)$  ( $\theta \in \mathbb{R}$ ) using its unbiased estimator  $\hat{f}(\theta)$ , i.e.,  $\langle \hat{f}(\theta) \rangle = f(\theta)$ . For simplicity, we first introduce one-dimensional case and then generalize that to two. The algorithm proceeds as follows for increasing  $f$ :

---

**Algorithm 1** Robbins Monro algorithm

---

**Input:**  $\theta_n$

1: sample  $x_n$  from  $\hat{f}(\theta_n)$

2:  $\theta_{n+1} \leftarrow \theta_n - a_n x_n$

**Output:**  $\theta_{n+1}$

---

where  $\{a_n\}_n$  is a slowly-decaying series of numbers which ensure the convergence; To be more specific,  $a_n > 0$  must satisfy  $\sum_n a_n = \infty$  and  $\sum_n a_n^2 < \infty$  [81]. As long as all the requirements are fulfilled,  $\theta_n$  converges to the root of  $f(\theta)$  with probability 1 regardless of the initial value  $\theta_1$ . Since concrete choice of  $a_n$  is left for us, we adopted the most conventional pattern:  $a_n = \frac{\alpha}{n}$  where  $\alpha > 0$  is a hyperparameter affecting the speed of convergence and fluctuation of  $\theta_n$ . What is more, as  $S(\beta, \Gamma)$ , which corresponds to  $f$  here, is by no means monotonic,  $\alpha$  also affects whether the algorithm converges or not. In the Appendix section, we will introduce a heuristic way of enchanting the robustness of the algorithm without impairing its performance.

For the multidimensional case, while a straightforward generalization based on a decaying series of diagonal matrices [54, 82] often works well, we can freely mix two independent feedbacks by introducing off-diagonal elements. It is notable that the optimal choice for  $a_n$ , this time it is a series of matrix, is  $[\nabla f(\theta^*)]^{-1}$  (inverse of the Jacobi matrix) where  $\theta^*$  is the root of  $f(\theta)$  [54], in terms of minimizing asymptotic variance of  $\theta_n$ . Hence nonzero off-diagonals are indeed beneficial in general. From the observation here, we further modified the target equation Eq. (11) and Eq. (12) as below,

$$S\left(0, \frac{2\pi i}{\beta}\right) - S\left(\frac{2\pi}{L}, 0\right) = 0, \quad (19)$$

$$S(0, 0) - \frac{1 + (2\pi R)^2}{2} \left[ S\left(0, \frac{2\pi i}{\beta}\right) + S\left(\frac{2\pi}{L}, 0\right) \right] = 0, \quad (20)$$

and tuned  $\beta$  by Eq. (19) and  $\Gamma$  by Eq. (20). In the physical view of point, Eq. (19) reads as aspect-ratio equality of  $\xi$ ,  $\xi_\beta$ , which we deduced that insensitive to  $\Gamma$ , and Eq. (20) as a constraint on averaged correlation length, which we assumed approximate independence of  $\beta$ . Two conjectures here are supported by numerical experiments, and thus we concluded that we can safely drop off-diagonal elements of  $a_n$  without harming performance, since  $\nabla f$  is approximately diagonal. As two diagonal elements are automatically tuned by the heuristics (see Appendix), we have no leftover hyperparameter.

## IV. RESULT

### A. data analysis

To get a data point for each  $(\sigma, L)$ , we iterated the Robbins-Monro update 100 times (10 sample per iteration) with the heuristics (see Appendix) as a burn-in process and approximated the target root  $(\beta(L), \Gamma(L))$  by the average of subsequent 2500 iterations together with its standard error calculated by binning analysis [45, 54, 83]. In the last stage, the heuristics were turned off.  $R$  was set different for each  $L$  so that  $\Gamma(L)$  quickly converges to  $\Gamma_c$ . Thanks to asymptotic  $R$  independence, we can directly compare the results even for different  $R$ . As for system size, we chose  $\text{round}(\sqrt{2}^n)$  ( $n = 6, 7, \dots, n_{\max}$ ) for each  $\sigma$ . Here  $n_{\max}$  is determined in terms of elapsed time, and thus it depends on  $\sigma$  since so the order of the algorithm does. After collecting all the data, we performed fitting based on Eqs. (II E). From this stage, though the sampler itself introduces no unpredictable errors, results suffer from finite-size artifacts originating from correction terms of the scaling relations, which persist sometimes even for the largest  $L$  in our simulations. To mitigate artifacts, we performed batched analysis, i.e., we grouped several sequential system sizes  $L_1, L_2, \dots, L_k$  (allow overlap) as a batch and checked the convergence of the results.  $k$  was chosen equal to the minimum reasonable value for each fit; For example, Eq. (15) requires  $k \geq 3$  hence we selected  $k = 3$ . Therefore, final error bars can be decomposed into statistical errors, finite-size artifacts, and fitting errors, which the second component was dominant for most of the cases. Note that we intentionally omitted the analyses of  $1/\nu$ , since three-parameter fitting to Eq. (16) is outstandingly unstable.

### B. exponents

Fig. 3 summarizes our results overlaid on theoretical predictions. For  $\sigma \leq \frac{2}{3}$ , our data look similar to the theoretical prediction (dotted line) even though they are not identical within error bars. The discrepancy is indeed *expected*, since the mean-field universality contains dangerous irrelevant variable  $u$  as discussed, and our method always extracts correction plus bare exponent. For the nontrivial  $\frac{2}{3} \leq \sigma \leq 2$ , exponents monotonically change as Ref. [36, 37, 41, 61]. There are no discernable anomalies near  $\sigma = 1$ , even though at this point the phase boundary of QPT marks the end of the KT transition (tricritical point). For  $\sigma \geq 2$ , obvious over/underestimates exist though the gap decreases as  $\sigma \rightarrow \infty$ . Unlike the previous case, the discrepancy is merely an artifact that may be attributed to the multiplicative logarithmic correction near the universality boundary. It is not clear whether the lower bound of the Ising universality is 2 or not, as the results here are dull even near  $\sigma = 2$ . In fact, in the nonuniversal re-

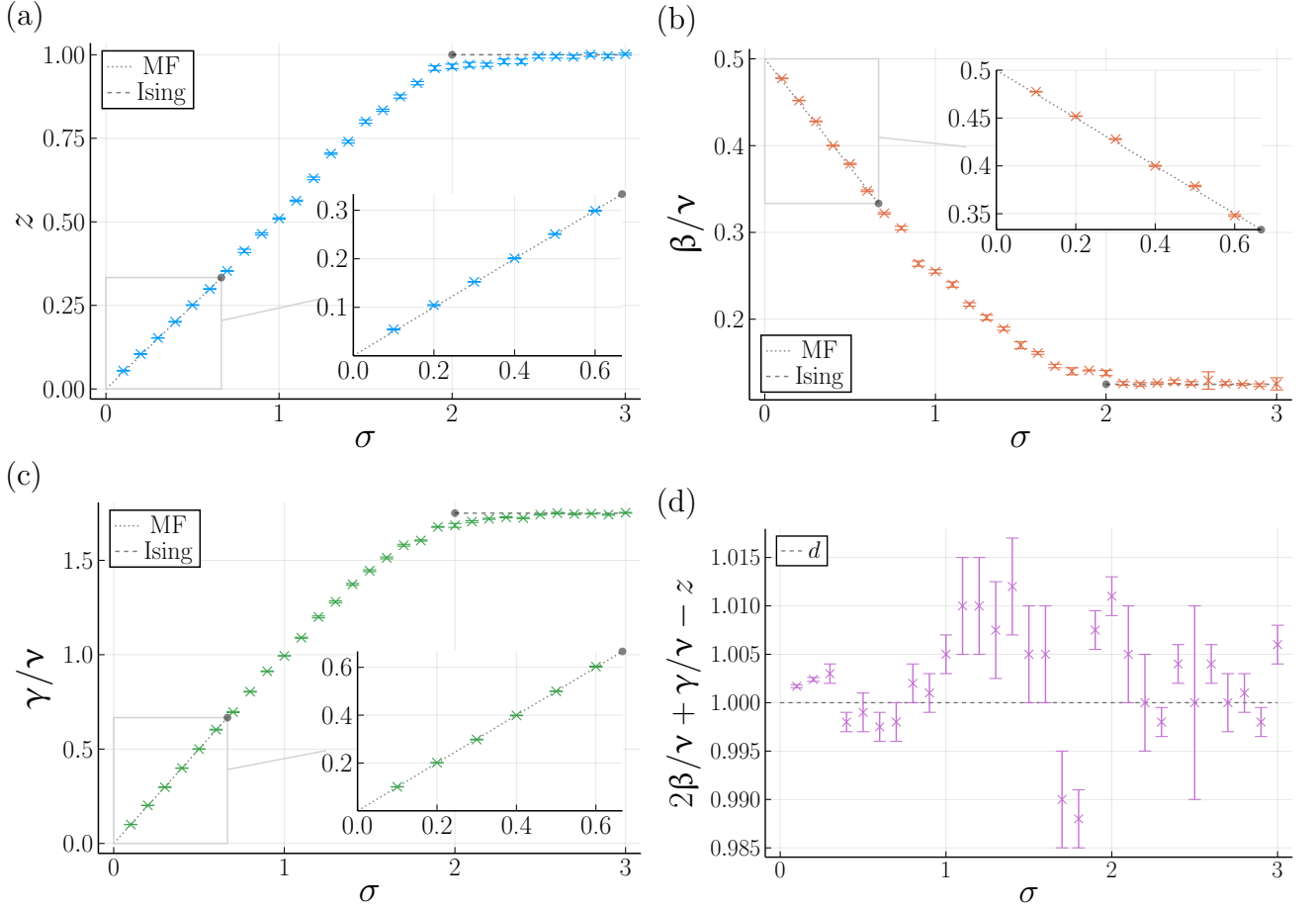


FIG. 3. (a): Dynamical critical exponent  $z$  estimated from  $\beta_c(L)$ . (b):  $\beta/\nu$  estimated from  $m^2$ . (c):  $\gamma/\nu$  estimated from  $S(0, 0)|_L$ . (d): Right-hand side of the hyperscaling relation  $2\beta/\nu + \gamma/\nu - z$ , which should be equal to  $d = 1$ . It implies that in the nonuniversal region ( $1 \lesssim \sigma \lesssim 2$ ) the results can contain severe finite-size artifacts.

gion ( $1 \lesssim \sigma \lesssim 2$ ) finite-size artifacts are notably severe (see Fig. IV B). To further investigate the topic, we will present another scheme next.

### C. validation analysis at $\sigma = 7/4$

We cannot conclude that the lower bound of the Ising universality is  $7/4$  (or not) from Fig. IV B. As an alternative, we performed a validation analysis at  $7/4$ , defined as follows; In the analysis, we fix  $\beta(L)$  as  $\beta = C_\beta L^{z'}$  where  $C_\beta > 0$  is an arbitrary constant,  $z'$  is an approximate of  $z$  guessed *a priori*. As we are focusing on the Ising universality here,  $z'$  is set to 1.  $\Gamma$  is still unspecified, and the Robbins-Monro algorithm decides it in reference to either Eq. (11) or Eq. (12). As we link either Eq. (11) or Eq. (12) to the Robbins-Monro algorithm, one of  $\xi$  or  $\xi_\beta$  is fixed to  $R$  while the other stays unbound. This time the heuristics were unnecessary because one-parameter tuning is more stable than two. Here we use 1000 iterations (10 samples per step as well) after first 100 deletion for each  $L$ .

Figure. 4 summarizes the result. It tells us that the unbound correlation lengths all converge to some constants for large  $L$ , even though they are completely excluded from the tuning process. This implies that if  $L$  is sufficiently large, we can draw a result that  $z = 1$  (Ising universality) from the two-parameter analysis at  $\sigma = 7/4$ . It is intriguing that the rates of convergence seem identical for six cases:  $\sim L^{-\frac{1}{2}}$ . It may be attributed to the fact that  $\xi/L$  and  $\xi_\beta/\beta$  are both convergent, and hence  $L^{-\frac{1}{2}}$  is the leading-order term of  $L$ -dependent corrections.

### D. critical field and phase diagram

Based on the discussions above, we came to the conclusion that the Ising universality seems to hold for  $\sigma \geq 7/4$ . Together with the analytical results for  $\sigma \leq 2/3$ , we drew the phase diagram of the model as Fig. 1. In the figure,  $\times$  symbols denote  $\Gamma_c$  estimated at  $\sigma = 0.1, 0.2, \dots, 3.0$  (see Appendix for data) and the curve is the cubic spline interpolation of the data. At  $\sigma = 1$ , QPT line and KT line meet at the tricritical point. For large  $\sigma$ ,  $\Gamma_c|_\sigma$  mono-

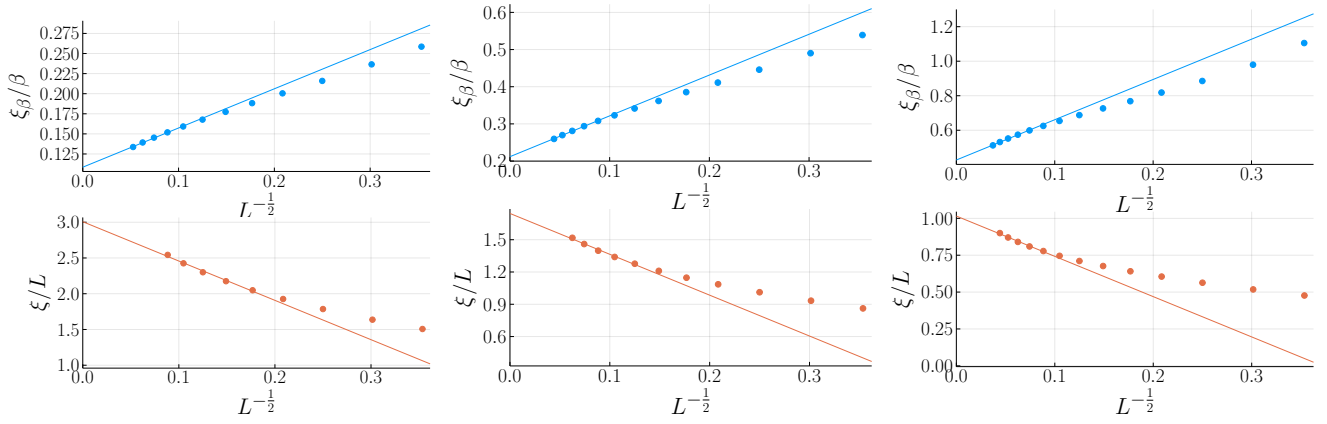


FIG. 4.  $L$  dependence of unbound correlation lengths, i.e., either  $\xi$  or  $\xi_\beta$  that the Robbins-Monro algorithm does not fix to  $R$ , measured under assumption that  $\beta(L)$  scales as  $C_\beta L^1$  (Ising universality). Three plots have different  $C_\beta$ : 19/25 (left), 19/50 (center), and 19/100 (right). They all converge to some constants for large  $L$ , implying that the Ising universality holds even at  $\sigma = 7/4 < 2$ .

tonically decreases to  $\simeq 1$ , which is the exact value for  $\sigma = \infty$  [45, 84]. In the opposite limit,  $\Gamma_c$  diverges as  $\sim \sigma^{-0.98(4)}$ . The result is comparable to Ref. [33], which states that  $\Gamma_c = \zeta(1+\sigma)$  (diverges as  $\sim \sigma^{-1}$  near +0 [85]) under an approximation.

## V. DISCUSSION

To begin with, let us summarize the results of this paper. For  $\sigma \leq 2/3$ , which is classified into the mean-field universality class, our method gives *different* results from the theoretical prediction as *expected*. This outcome might be interpreted as proof of the accuracy of the method, since it is aware of the corrections without any knowledge of the model. For nonuniversal  $2/3 \leq \sigma \lesssim 2$ , we observed monotonically varying exponents, which are consistent with previous studies [36, 37, 41, 61]. The upper bound of the nonuniversal region, which is under debate for now, is not clear from the two-parameter tuning analysis. As an auxiliary analysis, we performed a validation analysis at  $\sigma = 7/4$ , assuming that the Ising universality holds. The result states that the presumption is correct: we can surely conclude from the two-parameter analysis that the Ising universality governs  $\sigma = 7/4$  as long as  $L$  is sufficiently large, even though the required system size is unaffordable. For  $\sigma \gtrsim 2$ , while there exist obvious over/underestimates, the gap narrows as  $\sigma$  increases, and the exponents seem to converge to the analytical results for  $\sigma \rightarrow \infty$ . Even though our results contain several provisos mainly attributed to finite-size artifacts, they are consistent with the preceding results. Here we insist on Ref. [41] in relation to artifact reduction, which included nearest-neighbor interactions as distinct terms from long-range ones and adjusted the coupling strengths so that relevant interaction dominates the system. Although this procedure is not suitable for phase boundary determination, it has the potential to reduce

finite-size artifacts drastically.

Next, let us assess the method. In terms of computational cost, our method is obviously advantageous over ordinary MCMC: it requires only one simulation for each  $(\sigma, L)$  while conventional MCMC usually requires many data points from various  $(\beta, \Gamma)$ . This feature enables us to perform the exhaustive analysis evaluating 30 points, which is generally too expensive for MCMC analysis. Moreover, while the idea of scaling  $\beta$  as  $\sim L^z$  is already present [41], our method does not require  $z$  to be known in advance, achieving a fully automated analysis. As a consequence, our scheme requires no prior knowledge of the model. What is more, our framework, which couples MCMC and the Robbins-Monro algorithm, is widely applicable to various models with trivial modifications. For instance, consider the LRTFIM with spatial dimension higher than 1. Even for that case the Hamiltonian is parameterized by  $(\sigma, \Gamma, \beta)$ ; It clearly indicates that kernel codes for the Robbins-Monro algorithm are literally identical. For more conceptually different models we have to alter implementations, but the core scheme stays unchanged.

Before closing this paper, let us list possible improvements and future works. Currently we heavily rely on the heuristics in the tuning process, since two-parameter tuning is rather volatile. As a promising blueprint, we insist on an idea of additional dimension reduction based on the zero-temperature Monte Carlo method, which samples from the ground state distribution. With the algorithm,  $\Gamma$  is the only parameter fed to the Robbins-Monro optimizer. This can lead to massive improvements in stability, but we suspect sampling cost increase. On top of that, fitting analysis can also be a potential problem. Even though the simulation part introduces no unpredictable error in principle (provided the procedure converges), the analysis part suffers from severe finite-size corrections. As a countermeasure, we may utilize the remaining degrees of freedom (two  $R$ , target values of two



normalized  $\xi$ ) so that corrections are suppressed.

As closing remarks, let us locate our work. We invented a conceptually-different method based on MCMC, which requires less computations than ordinary schemes. We expect that it is especially powerful when one wants to perform exhaustive analyses of a model with additional degrees of freedom, long-ranged one is a chief example, and will be applied to other challenging models in the future.

## Appendix A: naive sampling algorithm

### 1. mapping to classical system

Using the Suzuki-Trotter decomposition [86], we first decompose partition function  $Z$  as

$$Z = \sum_{\{\Psi_t\}} \langle \Psi_1 | e^{-H\Delta\tau} | \Psi_2 \rangle \cdots \langle \Psi_m | e^{-H\Delta\tau} | \Psi_1 \rangle \quad (\text{A1})$$

where  $\Delta\tau$  is the discretization interval of the periodic imaginary-time axis  $\tau$ ,  $m = \frac{\beta}{\Delta\tau}$  is the number of slices, and  $|\Psi_t\rangle$  symbolically denotes a possible state at the  $t$  th slice: for spin- $\frac{1}{2}$  models such as the LRTFIM, one candidate of  $\{|\Psi\rangle\}$  is explicitly written as the union of all the possible  $L$  qubit bases  $\{|\sigma_1\rangle \otimes |\sigma_2\rangle \cdots |\sigma_L\rangle | \sigma_i \in \{\pm\}\}$ . This representation is the origin of many quantum Monte Carlo methods, including ours.

For the LRTFIM  $e^{-H\Delta\tau}$  is disassembled as

$$e^{-H\Delta\tau} \simeq \prod_{i < j} \exp[\Delta\tau J_{ij} \hat{\sigma}_i^z \hat{\sigma}_j^z] \prod_i \exp[\Delta\tau \Gamma \hat{\sigma}_i^x]. \quad (\text{A2})$$

This expression contains  $\mathcal{O}(\Delta\tau)$  errors originating from  $\hat{\sigma}^x$  and  $\hat{\sigma}^z$  being non-commutative. After substituting  $e^{-H\Delta\tau}$  with Eq. (A2) and  $|\Psi_t\rangle$  with the  $L$  qubit bases  $|\sigma_1^{(t)}\rangle \otimes |\sigma_2^{(t)}\rangle \cdots |\sigma_L^{(t)}\rangle$ , a new uniform nearest-neighbor interaction with its local Boltzmann weight equal to  $\langle \sigma^{(t)} | \exp[\Delta\tau \Gamma \hat{\sigma}^x] | \sigma^{(t+1)} \rangle$  appears as imaginary-time interactions. It is notable that this interaction is also Ising-like: by imposing  $e^{\Delta\tau \mathcal{J}} \propto \langle \pm | \exp[\Delta\tau \Gamma \hat{\sigma}^x] | \pm \rangle$  and  $e^{-\Delta\tau \mathcal{J}} \propto \langle \pm | \exp[\Delta\tau \Gamma \hat{\sigma}^x] | \mp \rangle$ , the coupling strength  $\mathcal{J}$  is obtained as  $\frac{1}{2\Delta\tau} \log[\coth \Delta\tau \Gamma]$ . After all, the discretized model is a two-dimensional ferromagnetic Ising model; For the  $x$  direction, the interactions are long-ranged, whereas for the  $\tau$  direction they are simple uniform nearest-neighbor ones.

### 2. naive sampling algorithm

Now that the model is reduced to a well-known Ising model, it is straightforward to sample from its corresponding canonical ensemble using MCMC. As the core algorithm, we adopted the Swendsen-Wang sampler [87]. For the  $\tau$  direction, the interactions are nearest-neighbor Ising ones parameterized by  $\mathcal{J}$ , which the original algorithm directly applies. An intriguing point here is that

the probability of connecting two adjacent aligned spins converges to 1 in the limit of  $\Delta\tau \rightarrow 0$ ; In the simulation, we consider its complementary event occurs with  $1 - p_{\text{bind}}^\tau \simeq \Delta\tau \Gamma$ . For the  $x$  direction, while the original algorithm only covers nearest-neighbor cases, we can extend it to long-ranged ones by considering long-ranged connections, i.e., cluster-merging events between  ${}_L C_2 = \mathcal{O}(L^2)$  pairs  $\{(i, j) | i < j\}$ . In contrast to the  $\tau$  direction, the probability of connection goes to 0:  $p_{\text{bind}}^x = 2\Delta\tau J_{ij}$ . Since the probabilities are  $\mathcal{O}(\Delta\tau)$  whereas the number of slices is  $m = \frac{\beta}{\Delta\tau} = \mathcal{O}(\Delta\tau^{-1})$ , we have finite number of events on average after taking  $\Delta\tau \rightarrow 0$  limit. In this limit, all the events are described by the Poisson process  $N(\rho, t)$  where  $\rho$  is probability density and  $t$  is the interval of the process.

It is convenient to introduce diagrammatic representation of the algorithm depicted as Fig. 5. In this formulation spin state  $\{\sigma_i^z(\tau) | i \in \mathbb{Z}_{[1, L)}, \tau \in [0, \beta), \sigma^z \in \{\pm\}\}$  are depicted as  $L$  vertical lines partitioned into black ( $|+1\rangle$ ) and red ( $|-1\rangle$ ) segments. The temporal periodicity, i.e.,  $|\Psi_{m+1}\rangle = |\Psi_1\rangle$  is reflected in both ends at  $\tau = (0, \beta)$  colored in the same color. Horizontal bars (solid, we call them “cut”) indicate where  $\mathcal{J}$  failed to bind, i.e., candidates of cluster boundary. Similarly, horizontal lines with circles (dotted, we call them “bind”) represent where  $J_{ij}$  successfully bound. Thanks to the original properties of the Swendsen-Wang algorithm,  $J_{ij}$  (dotted lines, “bind”) can only bind two same-color states, and kinks must coincide with rejected binding events of  $\mathcal{J}$  (solid black bars, “cuts”). These  $L + {}_L C_2$  types of graph elements (“cut” and “bind” between  $\{(i, j) | i < j\}$ )

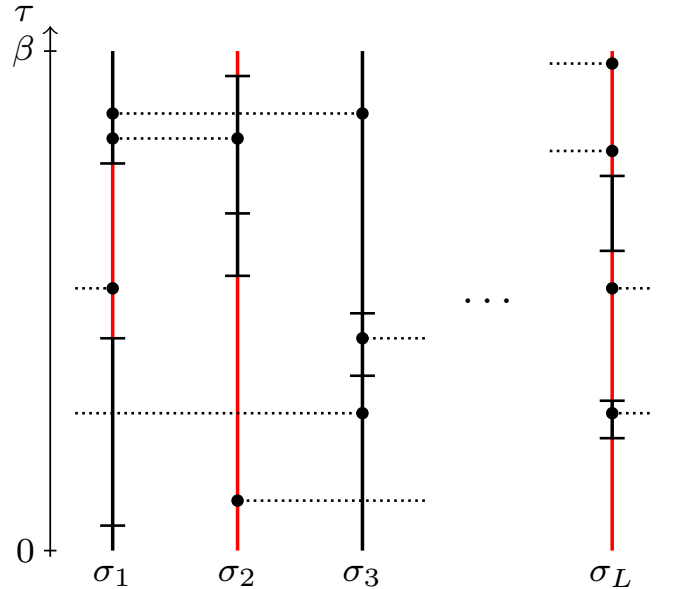


FIG. 5. Snapshot of the sampling process. Vertical lines represent a spin state, i.e.,  $|+1\rangle$  (black) or  $|-1\rangle$  (red), and horizontal solid/dashed lines correspond to the positions where the clusters are splitted/unified.



have corresponding Poisson processes which decide the positions of elements  $\tau \in [0, \beta)$ . For “cut” the process is  $N(\Gamma, \beta)$  regardless of  $i$ , and for “bind” the process is  $N(2J_{ij}, \beta)$ . After inserting graph elements, clusters are identified by the union-find algorithm [88] and each cluster gains a new random spin state. The full process, which costs  $\mathcal{O}(L^2)$  time, is summarized in Alg. 2. Note that conceptually we can sample any observable as a complete quantum state is explicitly stored, and using the graph itself we can indirectly measure several physical quantities more efficiently [45, 89, 90].

---

**Algorithm 2** naive algorithm

---

**Input:** initial state  
1: remove all “cut”  
2: **for all** kinks **do**  
3:   assign “cut” element  
4: **end for**  
5: **for**  $i$  **do**  
6:   sample  $T_{\text{cut}} \sim N(\Gamma, \beta)$   
7:   **for**  $\tau_{\text{cut}} \in T_{\text{cut}}$  **do**  
8:     assign “cut” to  $(x, \tau) = (i, \tau_{\text{cut}})$   
9:   **end for**  
10: **end for**  
11: **for**  $i < j$  **do**  
12:   sample  $T_{\text{bind}} \sim N(2J_{ij}, \beta)$   
13:   **for**  $\tau_{\text{bind}} \in T_{\text{bind}}$  **do**  
14:     **if**  $|\sigma_i^{(\tau)}\rangle = |\sigma_j^{(\tau)}\rangle$  **then**  
15:       assign “bind” between  $(i, \tau_{\text{cut}})$  and  $(j, \tau_{\text{cut}})$   
16:     **end if**  
17:   **end for**  
18: **end for**  
19: identify clusters  
20: **for all** clusters **do**  
21:   assign either  $|\pm\rangle$  at random  
22: **end for**  
**Output:** updated state

---

### 3. efficient algorithm

The bottleneck of the naive implementation is the sampling process from  ${}_LC_2$  different Poisson processes. As an improvement, we first fuse all the Poisson processes regarding particular cite  $i$  into one, explicitly denoted by  $N(\sum_{j \neq i} J_{ij} + \Gamma, \beta)$ . Here the factor 2 before  $\sum$  is intentionally erased by considering the rest half of  $\mathbb{Z}_{[0, L)}^2$  previously omitted, i.e.,  $\{(i, j) \mid i > j\}$ . After sampling from the fused process, the sampled event is distributed to one of  $L - 1$  independent “bind” or “cut” according to the weight  $\{J_{ij} \mid j \neq i\}$  and  $\Gamma$ . This reformation is known as thinning [49]; Informally speaking, it corresponds to postponing the decision of element type until the position is fixed. To implement this, we need to sample from  $L$ -element discrete distribution, which can be achieved in  $\mathcal{O}(1)$  time by the alias method [91]. The efficient algorithm is summarized in Alg. 3.

---

**Algorithm 3** efficient algorithm

---

**Input:** initial state  
1: remove all “cut”  
2: **for all** kinks **do**  
3:   assign “cut” element  
4: **end for**  
5: **for**  $i$  **do**  
6:   sample  $T \sim N(\sum_{j \neq i} J_{ij} + \Gamma, \beta)$   
7:   **for**  $\tau \in T$  **do**  
8:     sample element type from  $\propto \{J_{ij} \mid j \neq i\} \cup \{\Gamma\}$   
9:     **if**  $\Gamma$  (“cut”) is sampled **then**  
10:       assign “cut” to  $(x, \tau) = (i, \tau)$   
11:     **else if**  $J_{ij}$  (“bind”) is sampled **then**  
12:       assign “bind” between  $(i, \tau)$  and  $(j, \tau)$   
13:     **end if**  
14:   **end for**  
15: **end for**  
16: identify clusters  
17: **for all** clusters **do**  
18:   assign either  $|\pm\rangle$  at random  
19: **end for**  
**Output:** updated state

---

Note that, strictly speaking, this algorithm is not  $\mathcal{O}(L)$ ; In the clustering step, we have  $\mathcal{O}(L)$  singletons and need to perform  $\mathcal{O}(L)$  union-find operations. This costs  $\mathcal{O}(L\alpha(L))$  amortized time where  $\alpha$  is the inverse Ackermann function [92]. Although  $\alpha(L) \leq 4$  even for astronomically large  $L$ , it is still unbounded.

### Appendix B: more on the Robbins-Monro algorithm

The full process per iteration is summarized in Alg. 4.

---

**Algorithm 4** Robbins-Monro step

---

**Input:** initial  $(\beta, \Gamma, \alpha_\beta, \alpha_\Gamma, n)$   
1: sample  $S(0, 0), S(\frac{2\pi}{L}, 0), S(0, \frac{2\pi i}{\beta})$   
2: calculate  $f_\beta = S(0, 0) - [1 + (2\pi R)^2] S(0, \frac{2\pi i}{\beta})$   
3: calculate  $f_\Gamma = S(0, 0) - [1 + (2\pi R)^2] S(\frac{2\pi}{L}, 0)$   
4: **if** mixed scheme is used **then**  
5:    $(f_\beta, f_\Gamma) \leftarrow (\frac{1}{2}(f_\beta - f_\Gamma), \frac{1}{2}(f_\beta + f_\Gamma))$   
6: **end if**  
7:  $(f_\beta, f_\Gamma) \leftarrow (\frac{\alpha_\beta}{L\beta} f_\beta, \frac{\alpha_\Gamma}{L\beta} f_\Gamma)$   
8: adjust  $\alpha_\beta, \alpha_\Gamma$   
9:  $(f_\beta, f_\Gamma) \leftarrow (\frac{f_\beta}{n}, \frac{f_\Gamma}{n})$   
10: clamp  $f_\beta, f_\Gamma$   
11:  $(\beta, \Gamma) \leftarrow (\beta + f_\beta, \Gamma + f_\Gamma)$   
12: increment  $n$   
**Output:** updated  $(\beta, \Gamma, \alpha_\beta, \alpha_\Gamma, n)$

---

After sampling the required quantities (three  $S$ ), we first calculate the left-hand sides of Eq. (11) and Eq. (12). After that, two  $f$  are optionally mixed. This mixing stage typically reduces off-diagonal elements of the Jacobi matrix, which is beneficial for convergence as previously presented. Before applying the feedbacks, they are scaled by  $L\beta$  to avoid them from being too large;

The scaling factor is motivated by the asymptotic value of  $S(0, 0) \rightarrow L\beta$  near the absolute zero. From here, the procedures are straightforward other than two additional heuristic steps.

In the adjusting step, we increase or decrease  $\alpha_\theta$  ( $\theta = \beta, \Gamma$ ) depending on the relative amplitude of  $f_\theta$ . If  $|f_\theta/\theta| < c_\theta^{\text{inc}} = \frac{0.05}{3}$ , we increase  $\alpha_\theta$  by a factor of  $r = 1.01$ . Conversely  $\alpha_\theta$  is decreased by multiplying  $1/r$  when  $|f_\theta/\theta| > c_\theta^{\text{dec}} = 0.05$ . It is essential that two  $c_\theta$  are chosen so that  $c_\theta^{\text{inc}} < c_\theta^{\text{dec}}$ , otherwise  $\alpha_\theta$  will stray around the optimal value. Intuitively speaking, this step tries to adjust  $\alpha_\theta$  so that the parameter difference is  $\simeq \frac{0.05\theta}{n}$ .

In the clamping step, we limit  $f_\theta$  to  $[-c'_\theta\theta, c'_\theta\theta] = [-0.05\theta, 0.05\theta]$ . This procedure not only prevents  $\theta$  from being negative but also suppresses it from going too far away from the initial value. As the target function is not monotonic,  $\theta$  can even eagerly go away from the desired root without clamp once it escapes from the basin.

## ACKNOWLEDGMENTS

The computation in this paper has been done partly by Ohtaka supercomputer (ISSP, Univ. Tokyo) and nekoya/ai cluster (ipi, Univ. Tokyo).

- 
- [1] Y. Yamazaki, Critical exponent  $\eta$  of isotropic spin systems with long and short-range interactions, *Physics Letters A* **61**, 207 (1977).
  - [2] D. J. Thouless, Long-range order in one-dimensional ising systems, *Phys. Rev.* **187**, 732 (1969).
  - [3] M. Suzuki, Critical Exponents for Long-Range Interactions. II: Universality and Scaling Relations, *Progress of Theoretical Physics* **49**, 1106 (1973), <https://academic.oup.com/ptp/article-pdf/49/4/1106/5443731/49-4-1106.pdf>.
  - [4] J. Sak, Recursion Relations and Fixed Points for Ferromagnets with Long-Range Interactions, *Phys. Rev. B* **8**, 281 (1973).
  - [5] J. F. Nagle and J. C. Bonner, Numerical studies of the Ising chain with long-range ferromagnetic interactions, *Journal of Physics C: Solid State Physics* **3**, 352 (1970).
  - [6] H. Lipkin, N. Meshkov, and A. Glick, Validity of many-body approximation methods for a solvable model: (i). exact solutions and perturbation theory, *Nuclear Physics* **62**, 188 (1965).
  - [7] M. E. Fisher, S.-k. Ma, and B. G. Nickel, Critical exponents for long-range interactions, *Phys. Rev. Lett.* **29**, 917 (1972).
  - [8] S. A. Cannas, One-dimensional Ising model with long-range interactions: A renormalization-group treatment, *Phys. Rev. B* **52**, 3034 (1995).
  - [9] P. W. Anderson and G. Yuval, Some numerical results on the Kondo problem and the inverse square one-dimensional ising model, *Journal of Physics C: Solid State Physics* **4**, 607 (1971).
  - [10] S. T. Bramwell and M. J. P. Gingras, Spin ice state in frustrated magnetic pyrochlore materials, *Science* **294**, 1495 (2001), <https://www.science.org/doi/pdf/10.1126/science.1064761>.
  - [11] C. Castelnovo, R. Moessner, and S. L. Sondhi, Magnetic monopoles in spin ice, *Nature* **451**, 42 (2008).
  - [12] J. W. Britton, B. C. Sawyer, A. C. Keith, C.-C. J. Wang, J. K. Freericks, H. Uys, M. J. Biercuk, and J. J. Bollinger, Engineered two-dimensional ising interactions in a trapped-ion quantum simulator with hundreds of spins, *Nature* **484**, 489 (2012).
  - [13] R. Islam, C. Senko, W. C. Campbell, S. Korenblit, J. Smith, A. Lee, E. E. Edwards, C.-C. J. Wang, J. K. Freericks, and C. Monroe, Emergence and frustration of magnetism with variable-range interactions in a quantum simulator, *Science* **340**, 583 (2013), <https://www.science.org/doi/pdf/10.1126/science.1232296>.
  - [14] P. Jurcevic, B. P. Lanyon, P. Hauke, C. Hempel, P. Zoller, R. Blatt, and C. F. Roos, Quasiparticle engineering and entanglement propagation in a quantum many-body system, *Nature* **511**, 202 (2014).
  - [15] P. Richerme, Z.-X. Gong, A. Lee, C. Senko, J. Smith, M. Foss-Feig, S. Michalakis, A. V. Gorshkov, and C. Monroe, Non-local propagation of correlations in quantum systems with long-range interactions, *Nature* **511**, 198 (2014).
  - [16] J. G. Bohnet, B. C. Sawyer, J. W. Britton, M. L. Wall, A. M. Rey, M. Foss-Feig, and J. J. Bollinger, Quantum spin dynamics and entanglement generation with hundreds of trapped ions, *Science* **352**, 1297 (2016), <https://www.science.org/doi/pdf/10.1126/science.aad9958>.
  - [17] F. Yang, S.-J. Jiang, and F. Zhou, Achieving continuously tunable critical exponents for long-range spin systems simulated with trapped ions, *Phys. Rev. A* **99**, 012119 (2019).
  - [18] C. Monroe, W. C. Campbell, L.-M. Duan, Z.-X. Gong, A. V. Gorshkov, P. W. Hess, R. Islam, K. Kim, N. M. Linke, G. Pagano, P. Richerme, C. Senko, and N. Y. Yao, Programmable quantum simulations of spin systems with trapped ions, *Rev. Mod. Phys.* **93**, 025001 (2021).
  - [19] M. Saffman, T. G. Walker, and K. Mølmer, Quantum information with rydberg atoms, *Rev. Mod. Phys.* **82**, 2313 (2010).
  - [20] P. Schauß, M. Cheneau, M. Endres, T. Fukuhara, S. Hild, A. Omran, T. Pohl, C. Gross, S. Kuhr, and I. Bloch, Observation of spatially ordered structures in a two-dimensional rydberg gas, *Nature* **491**, 87 (2012).
  - [21] H. Labuhn, D. Barredo, S. Ravets, S. de Léséleuc, T. Macrì, T. Lahaye, and A. Browaeys, Tunable two-dimensional arrays of single rydberg atoms for realizing quantum ising models, *Nature* **534**, 667 (2016).
  - [22] R. Landig, L. Hruby, N. Dogra, M. Landini, R. Mottl, T. Donner, and T. Esslinger, Quantum phases from competing short- and long-range interactions in an optical lattice, *Nature* **532**, 476 (2016).
  - [23] A. Browaeys and T. Lahaye, Many-body physics with individually controlled rydberg atoms, *Nature Physics* **16**, 132 (2020).
  - [24] S. Fey and K. P. Schmidt, Critical behavior of quantum magnets with long-range interactions in the thermody-

- namic limit, Phys. Rev. B **94**, 075156 (2016).
- [25] S. Fey, S. C. Kapfer, and K. P. Schmidt, Quantum Criticality of Two-Dimensional Quantum Magnets with Long-Range Interactions, Phys. Rev. Lett. **122**, 017203 (2019).
  - [26] P. Adelhardt, J. A. Koziol, A. Schellenberger, and K. P. Schmidt, Quantum criticality and excitations of a long-range anisotropic XY chain in a transverse field, Phys. Rev. B **102**, 174424 (2020).
  - [27] M. Knap, A. Kantian, T. Giamarchi, I. Bloch, M. D. Lukin, and E. Demler, Probing Real-Space and Time-Resolved Correlation Functions with Many-Body Ramsey Interferometry, Phys. Rev. Lett. **111**, 147205 (2013).
  - [28] A. W. Sandvik, Ground states of a frustrated quantum spin chain with long-range interactions, Phys. Rev. Lett. **104**, 137204 (2010).
  - [29] P. Hauke and M. Heyl, Many-body localization and quantum ergodicity in disordered long-range ising models, Phys. Rev. B **92**, 134204 (2015).
  - [30] H. Li, J. Wang, X.-J. Liu, and H. Hu, Many-body localization in ising models with random long-range interactions, Phys. Rev. A **94**, 063625 (2016).
  - [31] I. Homrighausen, N. O. Abeling, V. Zauner-Stauber, and J. C. Halimeh, Anomalous dynamical phase in quantum spin chains with long-range interactions, Phys. Rev. B **96**, 104436 (2017).
  - [32] Z. Zhu, G. Sun, W.-L. You, and D.-N. Shi, Fidelity and criticality of a quantum Ising chain with long-range interactions, Phys. Rev. A **98**, 023607 (2018).
  - [33] D. Jaschke, K. Maeda, J. D. Whalen, M. L. Wall, and L. D. Carr, Critical phenomena and kibble-zurek scaling in the long-range quantum ising chain, New Journal of Physics **19**, 033032 (2017).
  - [34] F. Fröwis, V. Nebendahl, and W. Dür, Tensor operators: Constructions and applications for long-range interaction systems, Phys. Rev. A **81**, 062337 (2010).
  - [35] V. Murg, F. Verstraete, O. Legeza, and R. M. Noack, Simulating strongly correlated quantum systems with tree tensor networks, Phys. Rev. B **82**, 205105 (2010).
  - [36] N. Defenu, A. Trombettoni, and S. Ruffo, Criticality and phase diagram of quantum long-range  $O(n)$  models, Phys. Rev. B **96**, 104432 (2017).
  - [37] J. A. Koziol, A. Langheld, S. C. Kapfer, and K. P. Schmidt, Quantum-critical properties of the long-range transverse-field Ising model from quantum Monte Carlo simulations, Phys. Rev. B **103**, 245135 (2021).
  - [38] A. W. Sandvik, Stochastic series expansion method for quantum Ising models with arbitrary interactions, Phys. Rev. E **68**, 056701 (2003).
  - [39] E. G. Lazo, M. Heyl, M. Dalmonte, and A. Angelone, Finite-temperature critical behavior of long-range quantum Ising models, SciPost Phys. **11**, 076 (2021).
  - [40] I. B. Sperstad, E. B. Stiansen, and A. Sudbø, Monte carlo simulations of dissipative quantum ising models, Phys. Rev. B **81**, 104302 (2010).
  - [41] I. B. Sperstad, E. B. Stiansen, and A. Sudbø, Quantum criticality in spin chains with non-ohmic dissipation, Phys. Rev. B **85**, 214302 (2012).
  - [42] S. Humeniuk, Quantum monte carlo study of long-range transverse-field ising models on the triangular lattice, Phys. Rev. B **93**, 104412 (2016).
  - [43] S. Humeniuk, Thermal kosterlitz-thouless transitions in the  $1/r^2$  long-range ferromagnetic quantum ising chain revisited, Journal of Statistical Mechanics: Theory and Experiment **2020**, 063105 (2020).
  - [44] S. R. White, Density matrix formulation for quantum renormalization groups, Phys. Rev. Lett. **69**, 2863 (1992).
  - [45] J. Gubernatis, N. Kawashima, and P. Werner, *Quantum Monte Carlo Methods: Algorithms for Lattice Models* (Cambridge University Press, 2016).
  - [46] G. M. Crosswhite, A. C. Doherty, and G. Vidal, Applying matrix product operators to model systems with long-range interactions, Phys. Rev. B **78**, 035116 (2008).
  - [47] B. Pirvu, V. Murg, J. I. Cirac, and F. Verstraete, Matrix product operator representations, New Journal of Physics **12**, 025012 (2010).
  - [48] K. Fukui and S. Todo, Order-N cluster Monte Carlo method for spin systems with long-range interactions, Journal of Computational Physics **228**, 2629 (2009).
  - [49] J. F. C. Kingman, *Poisson processes*, Vol. 3 (Clarendon Press, 1992).
  - [50] D. P. Landau and K. Binder, *A Guide to Monte Carlo Simulations in Statistical Physics*, 4th ed. (Cambridge University Press, 2014).
  - [51] K. Binder, M. Nauenberg, V. Privman, and A. P. Young, Finite-size tests of hyperscaling, Phys. Rev. B **31**, 1498 (1985).
  - [52] K. Binder, Finite size effects on phase transitions, Ferroelectrics **73**, 43 (1987), <https://doi.org/10.1080/00150198708227908>.
  - [53] H. Robbins and S. Monro, A Stochastic Approximation Method, The Annals of Mathematical Statistics **22**, 400 (1951).
  - [54] S. Yasuda, H. Suwa, and S. Todo, Stochastic approximation of dynamical exponent at quantum critical point, Phys. Rev. B **92**, 104411 (2015).
  - [55] S. Sachdev, *Quantum Phase Transitions*, 2nd ed. (Cambridge University Press, 2011).
  - [56] A. Dutta and J. K. Bhattacharjee, Phase transitions in the quantum Ising and rotor models with a long-range interaction, Phys. Rev. B **64**, 184106 (2001).
  - [57] E. Luijten and H. Meßingfeld, Criticality in One Dimension with Inverse Square-Law Potentials, Phys. Rev. Lett. **86**, 5305 (2001).
  - [58] A. Campa, T. Dauxois, and S. Ruffo, Statistical mechanics and dynamics of solvable models with long-range interactions, Physics Reports **480**, 57 (2009).
  - [59] A. Campa, T. Dauxois, D. Fanelli, and S. Ruffo, *Physics of Long-Range Interacting Systems* (Oxford University Press, 2014).
  - [60] E. Luijten and H. W. J. Blöte, Classical critical behavior of spin models with long-range interactions, Phys. Rev. B **56**, 8945 (1997).
  - [61] R. Puebla, O. Marty, and M. B. Plenio, Quantum kibble-zurek physics in long-range transverse-field ising models, Phys. Rev. A **100**, 032115 (2019).
  - [62] L. Onsager, Crystal Statistics. I. A Two-Dimensional Model with an Order-Disorder Transition, Phys. Rev. **65**, 117 (1944).
  - [63] C. N. Yang, The Spontaneous Magnetization of a Two-Dimensional Ising Model, Phys. Rev. **85**, 808 (1952).
  - [64] M. Suzuki and G. Igarashi, Calculation of Critical Slowing Down Exponent Using Wilson's Expansion Methods, Progress of Theoretical Physics **49**, 1070 (1973), <https://academic.oup.com/ptp/article-pdf/49/3/1070/5261146/49-3-1070.pdf>.
  - [65] M. Picco, Critical behavior of the ising model with long range interactions (2012), arXiv:1207.1018 [cond-mat.stat-mech].

- [66] T. Blanchard, M. Picco, and M. A. Rajabpour, Influence of long-range interactions on the critical behavior of the ising model, *Europhysics Letters* **101**, 56003 (2013).
- [67] P. Grassberger, Two-dimensional sir epidemics with long range infection, *Journal of Statistical Physics* **153**, 289 (2013).
- [68] G. Gori, M. Michelangeli, N. Defenu, and A. Trombettoni, One-dimensional long-range percolation: A numerical study, *Phys. Rev. E* **96**, 012108 (2017).
- [69] E. Luijten and H. W. J. Blöte, Boundary between long-range and short-range critical behavior in systems with algebraic interactions, *Phys. Rev. Lett.* **89**, 025703 (2002).
- [70] M. C. Angelini, G. Parisi, and F. Ricci-Tersenghi, Relations between short-range and long-range ising models, *Phys. Rev. E* **89**, 062120 (2014).
- [71] T. Horita, H. Suwa, and S. Todo, Upper and lower critical decay exponents of ising ferromagnets with long-range interaction, *Phys. Rev. E* **95**, 012143 (2017).
- [72] M. F. Paulos, S. Rychkov, B. C. van Rees, and B. Zan, Conformal invariance in the long-range ising model, *Nuclear Physics B* **902**, 246 (2016).
- [73] C. Behan, L. Rastelli, S. Rychkov, and B. Zan, A scaling theory for the long-range to short-range crossover and an infrared duality\*, *Journal of Physics A: Mathematical and Theoretical* **50**, 354002 (2017).
- [74] C. Behan, L. Rastelli, S. Rychkov, and B. Zan, Long-Range Critical Exponents near the Short-Range Crossover, *Phys. Rev. Lett.* **118**, 241601 (2017).
- [75] C. Behan, Bootstrapping the long-range ising model in three dimensions, *Journal of Physics A: Mathematical and Theoretical* **52**, 075401 (2019).
- [76] E. J. Flores-Sola, B. Berche, R. Kenna, and M. Weigel, Finite-size scaling above the upper critical dimension in ising models with long-range interactions, *The European Physical Journal B* **88**, 28 (2015).
- [77] B. Berche, R. Kenna, and J.-C. Walter, Hyperscaling above the upper critical dimension, *Nuclear Physics B* **865**, 115 (2012).
- [78] D. Vodola, L. Lepori, E. Ercolessi, and G. Pupillo, Long-range Ising and Kitaev models: phases, correlations and edge modes, *New Journal of Physics* **18**, 015001 (2015).
- [79] L. Vanderstraeten, M. Van Damme, H. P. Büchler, and F. Verstraete, Quasiparticles in Quantum Spin Chains with Long-Range Interactions, *Phys. Rev. Lett.* **121**, 090603 (2018).
- [80] F. Cooper, B. Freedman, and D. Preston, Solving  $\varphi_{1,2}^4$  field theory with Monte Carlo, *Nuclear Physics B* **210**, 210 (1982).
- [81] C. Bishop, *Pattern Recognition and Machine Learning: All "just the Facts 101" Material*, Information science and statistics (Springer (India) Private Limited, 2013).
- [82] J. R. Blum, Multidimensional Stochastic Approximation Methods, *The Annals of Mathematical Statistics* **25**, 737 (1954).
- [83] M. Wallerberger, S. Isakov, A. Gaenko, J. Kleinhenz, I. Krivenko, R. Levy, J. Li, H. Shinaoka, S. Todo, T. Chen, X. Chen, J. P. F. LeBlanc, J. E. Paki, H. Terletskaya, M. Troyer, and E. Gull, Updated core libraries of the alps project (2018), arXiv:1811.08331 [physics.comp-ph].
- [84] E. Lieb, T. Schultz, and D. Mattis, Two soluble models of an antiferromagnetic chain, *Annals of Physics* **16**, 407 (1961).
- [85] E. T. Whittaker and G. N. Watson, The Zeta Function of Riemann, in *A Course of Modern Analysis*, Cambridge Mathematical Library (Cambridge University Press, 1996) pp. 265–280, 4th ed.
- [86] M. Suzuki, Relationship between d-Dimensional Quantum Spin Systems and (d+1)-Dimensional Ising Systems: Equivalence, Critical Exponents and Systematic Approximants of the Partition Function and Spin Correlations, *Progress of Theoretical Physics* **56**, 1454 (1976), <https://academic.oup.com/ptp/article-pdf/56/5/1454/5264429/56-5-1454.pdf>.
- [87] R. H. Swendsen and J.-S. Wang, Nonuniversal critical dynamics in Monte Carlo simulations, *Phys. Rev. Lett.* **58**, 86 (1987).
- [88] B. A. Galler and M. J. Fischer, An improved equivalence algorithm, *Commun. ACM* **7**, 301 (1964).
- [89] U. Wolff, Collective monte carlo updating for spin systems, *Phys. Rev. Lett.* **62**, 361 (1989).
- [90] A. Avella and F. Mancini, *Strongly Correlated Systems: Numerical Methods*, Springer Series in Solid-State Sciences (Springer Berlin Heidelberg, 2013).
- [91] A. J. Walker, An efficient method for generating discrete random variables with general distributions, *ACM Trans. Math. Softw.* **3**, 253 (1977).
- [92] T. H. Cormen, C. E. Leiserson, R. L. Rivest, and C. Stein, *Introduction to Algorithms, Third Edition*, 3rd ed. (The MIT Press, 2009).